Soft Matter

PAPER

View Article Online
View Journal | View Issue



Cite this: *Soft Matter*, 2014, **10**, 6749

# Environmentally responsive polymeric materials: effect of the topological structure on self-assembly†

Hui Wang,[a] Pei Zhang,[a] Xuefeng Shi,[a] Danfeng Yu,[a] Jinben Wang,*[a] Haike Yan[a] and Gang Ji[b]

Received 16th May 2014
Accepted 24th June 2014

DOI: 10.1039/c4sm01072h

www.rsc.org/softmatter

A novel amphiphilic homopolymer ($PAGC_8$), containing two hydrophilic head groups and double hydrophobic tails in each repeat unit, has been prepared by solution polymerization and named as "a geminized amphiphilic homopolymer" in this paper, which is capable of self-assembling into various nanoobjects depending on the solution concentration and solvent properties. Characterization of the self-assembly behaviors was carried out by steady-state fluorescence, transmission electron microscopy and nuclear magnetic resonance techniques. Particular emphasis was dedicated to the environmental responsiveness of the assemblies. The morphologies were observed to transform from micelle-type to vesicles on adding a certain amount of ethanol. It is noteworthy that the assemblies were able to trap hydrophilic (rhodamine B) and hydrophobic (Sudan Red) molecules. Subsequently different nanoobjects were found after the encapsulation. To probe the effect of the topological structure on the self-assembly behaviors, the properties of an additional homopolymer with single charge pendant architecture on the backbone were investigated for comparison. Significant differences in structure between the two architectures brought out remarkable variations in aggregates, which were non-responsive to the solvent environment, or encapsulation of molecules. Based on the experimental results, we proposed a possible mechanism of the morphological transitions of the assemblies.



## 1. Introduction

Amphiphilic polymers are broadly classified into homopolymers and block, random, alternate, and graft copolymers.[1] Recent studies have shown that the hydrophobic blocks of amphiphilic multiblock copolymers tend to aggregate, while the hydrophilic blocks tend to dissolve in a dilute aqueous solution. These two competitive effects lead to the formation of unique micelle structures, such as spheres, rods, bowl-like micelles, large compound vesicles, *etc.*[2–4] Amphiphilic homopolymers, in which each repeat unit contains a hydrophilic head group and hydrophobic tail, have been increasing in number in recent years due to their facile synthesis and the capability of providing diverse self-assembled structures.[1,5–10] In view of fuzzy hydrophobic and hydrophilic boundaries, homopolymers are very different from their block copolymer analogues in the aggregation behaviors and aggregate structures. Namely, homopolymers with the best defined molecular structure and simple composition have significant advantages that the factors of covalently linked structures exist in the supramolecular assemblies, and therefore, the thermodynamic stability is higher.[11] Meanwhile, the aggregates can be unimolecular micelles, or a core with a large space formed by several molecules, which signifies their good solubilization to be used as supramolecular hosts.[12,13] Pioneering studies have been explored by Thayumanavan *et al.*, in which a type of homopolymer possessing a relatively long hydrophobic side chain and a short hydrophilic carboxylic acid group in every repeat unit was prepared and was able to form a micelle-like structure.[14] Subsequently, the author discovered that a range of amphiphilic homopolymers with high hydrophobic content could self-assemble into hollow aggregates and spherical micelles possessing low hydrophobic content in water.[15] Shunmugam *et al.* obtained polymersomes using self-assembly of amphiphilic homopolymers with unique structure which could be used as a nano-reservoir for controlled release of doxorubicin.[16]

Given the enhanced stability of assemblies and their usage in a variety of applications for amphiphilic homopolymers,[17–19] we focused on the electrostatic and hydrophobic interactions as a means of controlling the self-assembly behaviors. One of the main concerns is to utilize the unique structure to regulate the

[a]*Key Laboratory of Colloid and Interface Science, Beijing National Laboratory for Molecular Sciences (BNLMS), Institute of Chemistry, Chinese Academy of Sciences, Beijing 100190, P. R. China. E-mail: jbwang@iccas.ac.cn; Fax: +86-10-62523395; Tel: +86-10-62523395*

[b]*Center for Biological Electron Microscopy, Institute of Biophysics, Chinese Academy of Sciences, Beijing 100101, P. R. China*

† Electronic supplementary information (ESI) available: Characterization data of homopolymers $PAGC_8$ and $PASC_8$ by $^1H$ NMR, GPC, and TEM images of monomer $AGC_8$ in water and ethanol. See DOI: 10.1039/c4sm01072h

self-assembly to obtain well-defined nanoobjects in water or organic solvents. On the other hand, the self-assembled structures are promising platforms to trap a variety of molecules, which may offer applications as nanocarriers.

In previous work, we designed a class of amphiphilic copolymers partly containing gemini surfactant segments, which showed superior surface activity and various self-assembly behaviors compared to those of their counterparts without gemini type surfactant units.[20] In consequence, the amphiphilic homopolymer purely composed of gemini surfactant segments, namely, containing two hydrophilic head groups and hydrophobic tails in each repeat unit will possess exceptional properties and perform remarkably in the molecular aggregation processes. This kind of amphiphilic homopolymer is promising for expanding the scope of "smart" materials. Based on the above assumption, the geminized amphiphilic homopolymer, poly-1,3-bis (*N*,*N*-dimethyl-*N*-octylammonium)-2-propylacrylate dibromide (referred to as $PAGC_8$), was synthesized by polymerization of the corresponding gemini surfactant monomer, and its aggregation behaviors were also investigated. For comparison, another traditional amphiphilic homopolymer, comprising one hydrophilic head group and a single hydrophobic tail in each repeat unit (poly-acryloyloxyethyl-*N*,*N*-dimethyl-*N*-octylammonium bromide, referred to as $PASC_8$), was prepared and the investigation on its molecular self-assembly behaviors was also carried out parallelly. On the basis of characterization data, we discussed the molecular association mechanism, aggregate structures and the effect of solvent polarity on the aggregation behaviors.

## 2. Experimental section

### 2.1 Materials

Pyrene was purchased from Aldrich and recrystallized from ethanol. Deuterium oxide (99.9%), chloroform-d (99.9%) and ethanol-d6 (99%) were purchased from Acros. Acryloyl chloride, 1-bromine octane, ammonium persulfate, ammonium iron[II] sulfate hexahydrate and solvents were purchased from Beijing Chemical Co. (A.R. Grade). All reagents except those especially mentioned were used without further purification. The intermediate compounds acryloyloxyethyl-*N*,*N*-dimethyl-*N*-octylammonium bromide (abbreviated as $ASC_8$)[21] and 1,3-bis(*N*,*N*-dimethyl-*N*-octyl ammonium)-2-hydroxylpropane dibromide[22] (abbreviated as BHD-$C_8$) were prepared according to previously reported literature. All solutions were prepared with Milli-Q gradient ultra pure water.

### 2.2 Synthesis

The synthetic route and the structure of geminized homopolymer $PAGC_8$ are shown in Fig. 1.

**2.2.1 Synthesis of monomer ($AGC_8$).** The monomer was prepared by reaction of acryloyl chloride with BHD-$C_8$ (see step 2 in Fig. 1). Acryloyl chloride (5.43 g, 0.06 mol) was added dropwise to an anhydrous chloroform solution of BHD-$C_8$ (26.6 g, 0.05 mol) in 50 mL dichloromethane solution with triethylamine (0.06 mol), which was kept at 0 °C by cooling with an external ice bath. After complete addition of acryloyl chloride, the mixture was stirred for 1 h, and then the temperature was allowed to rise to 40 °C under stirring for 24 h. After removing the solvents by evaporation under reduced pressure, the residue was dissolved in acetone and filtered. The filtrate was recrystallized from acetone/diethyl ether repeatedly to afford a white solid. $^1$H NMR (400 MHz, $CDCl_3$): $\delta$ 0.87 (6H, t, $-CH_2-CH_3$), 1.26–1.34 (20H, m, $-(CH_2)_5-$), 1.74–1.80 (4H, m, $-N-CH_2-CH_2$), 3.42–3.50 (12H, d, $N-(CH_3)_2$), 3.56 (4H, m, $N-CH_2-$), 4.63–4.69 (2H, m, $N-CH_2-CH$), 4.87 (2H, d, $N-CH_2-CH$), 5.99 (1H, d, $CH_2=CH-$), 6.16–6.26 (1H, q, $CH_2=CH-$), 6.37 (1H, m, O–CH–), 6.89–6.93 (1H, d, $CH_2=CH-$).

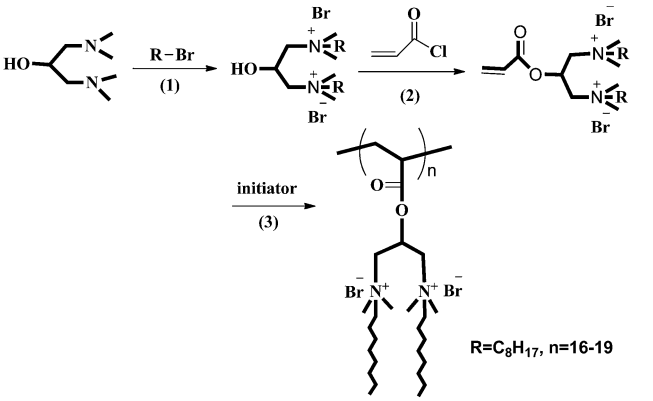


Fig. 1 Synthesis and structure of geminized homopolymer $PAGC_8$.

**2.2.2 Synthesis of homopolymers $PAGC_8$ and $PASC_8$.** Amphiphilic homopolymers poly-1,3-bis(*N*,*N*-dimethyl-*N*-octylammonium)-2-propylacrylate dibromide ($PAGC_8$) and poly-acryloyloxyethyl-*N*,*N*-dimethyl-*N*-octylammonium bromide ($PASC_8$) were prepared by free radical polymerization in aqueous solution at 10 °C, using ammonium persulfate and ammonium iron[II] sulfate hexahydrate as initiators, as shown in Fig. 1. The monomer $AGC_8$ (5.86 g, 0.01 mol) or $ASC_8$ (5.32 g, 0.01 mol) aqueous solution (20% solid content, wt%) was added into a 50 mL glass reactor equipped with a magnetic stirrer, thermometer, gas inlet, and water-bath thermostat. Before polymerization, the solution was bubbled with nitrogen ($N_2$) for 0.5 h to remove oxygen ($O_2$). Then the initiators (0.05% in the mixture) were added successively at 10 °C. The polymerization was allowed to proceed for 2 h under a $N_2$ atmosphere. The products were dialyzed against pure water using a membrane with a molecular weight cutoff of 3.5 kDa for 6 days, and the final homopolymers were obtained by lyophilization. It can be seen from the results of $^1$H NMR and GPC (see ESI Fig. S1 and Table S1†) that homopolymers $PAGC_8$ and $PASC_8$ were successfully synthesized with $M_w$ being about $1.1 \times 10^4$ Da.

### 2.3 Encapsulation procedure of aggregates

1 mL rhodamine B (Sudan Red) at a concentration of 1 g $L^{-1}$ was added dropwise to $PAGC_8$/$PASC_8$ (10 g $L^{-1}$, 1 mL) aqueous solution with slight stirring. The solution was then dialyzed against water (Sudan Red in ethanol) using a membrane with a molecular weight cutoff of 3.5 kDa for 6 days to remove non-

trapped molecules. The morphological analysis of the dialyzed solutions was then performed by CLSM and TEM on samples stained by uranyl acetate.

### 2.4 Measurements

**2.4.1 Nuclear magnetic resonance (NMR).** All $^1$H NMR measurements were carried out at 25.0 ± 0.1 °C on a Bruker AV500 FT-NMR spectrometer (500.1 MHz). Deuterium oxide and ethanol-d6 were used to prepare the sample solutions. Considering the variation of chemical shifts in different solvents, chloroform-d in the same capillary was used as an external standard. $T_1$ (spin–lattice) and $T_2$ (spin–spin) relaxation times were determined, using inversion recovery and CPMG pulse sequences, respectively.

**2.4.2 Gel permeation chromatography (GPC).** The homopolymer molecular weights and polydispersities were determined using a Waters Breeze 1515 GPC analysis system (DMF). The homopolymers were dissolved in DMF and filtered prior to analysis.

**2.4.3 Steady-state fluorescence.** Pyrene was employed as a fluorescence probe at a concentration of 1 μM and the sample solutions were stirred at room temperature overnight before measurement. Steady-state fluorescence spectra were obtained with a Hitachi F-4500 spectrofluorometer at 25.0 ± 0.5 °C. The emission spectra were scanned from 350 to 550 nm using a 335 nm excitation wavelength. The width of the emission slit was 2.5 nm.

**2.4.4 Confocal laser scanning microscopy (CLSM).** Images captured using a Confocal Laser Scanning Microscope (CLSM) were analysed using a confocal laser scanning biological microscope (FV1000-IX81, Olympus, Japan) using a 559 nm laser (FV5-LAMAR) and the fluorescence was highlighted in red.

**2.4.5 Transmission electron microscopy (TEM).** The operation was performed under a JEM-1011 electron microscope at a working voltage of 100 kV. Each sample solution (3 μL) was dropped onto a carbon-coated grid (300 meshes) and dried at an ambient environment. To stain those aggregates, uranyl acetate solution (0.5%) was dropped onto a hydrophobic film (Parafilm), and then those sample-loaded grids were laid upside down on the top of the droplet for 3–6 min. After that a filter paper was used to carefully blot the excess solution. The grids were dried under an ambient environment overnight.

**2.4.6 Cryogenic transmission electron microscopy (Cryo-TEM).** The Cryo-TEM results are capable of reflecting the aggregate morphology in solution and overcoming the illusions from the preparation process. The sample was embedded in a thin layer of vitreous ice on freshly carbon-coated holey TEM grids by blotting the grids with filter paper and then plunging them into liquid ethane cooled by liquid nitrogen. Frozen hydrated specimens were imaged by using an FEI Tecnai 20 electron microscope (LaB6) operating at 200 kV in the low-dose mode (about 2000 e per nm$^2$) and the nominal magnification of 50 000. For each specimen area, the defocus was set to 1–2 μm. Images were recorded on Kodak SO163 films and then digitized using a Nikon 9000 with a scanning step of 2000 dpi corresponding to 2.54 Å per pixel.

**2.4.7 Electrical conductivity.** The conductivity of the homopolymer solutions was measured as a function of concentration using a JENWAY model 4320 conductivity meter, performing in a temperature-controlled, double-walled glass container with a circulation of water. A sufficient time was allowed for equilibrium between successive additions. The temperature of the solution was controlled at 25.0 ± 0.1 °C.

## 3. Results and discussion

### 3.1 The aggregation behaviors of homopolymers in aqueous solution

The cac of amphiphilic homopolymers is an important parameter for characterizing their self-assembly in aqueous solution. The steady-state fluorescence with pyrene as a probe is frequently and effectively used to measure the cac of amphiphilic polymers. The emission and excitation spectra of pyrene are sensitive to the microenvironment polarity. In emission spectra, the relative intensities of the first vibronic peak ($I_1$) and the third vibronic peak ($I_3$) are sensitive to the environment polarity, which are frequently used for the determination of aggregate polarity and critical micelle concentration.[23,24]

Fig. 2 shows variations of intensity ratio $I_1/I_3$ *versus* the concentration of $PAGC_8$ and $PASC_8$ in aqueous solution. The plots have a usual sigmoid shape with a rapid decrease of $I_1/I_3$ at measured concentration. With the increase of concentration, the $I_1/I_3$ ratios of $PAGC_8$ decreased sharply while those of $PASC_8$ decreased tardily after a certain concentration region, showing significant variation in the polarity of the hydrophobic microdomain and little difference in the cac value. Similar cac values are not consistent with the previous studies that amphiphilic copolymers containing gemini surfactant units have lower cac values than those of polymers comprising traditional single-tailed surfactant segments.[20] The probable reason may be related to the topology structure of the homopolymers. The two alkyl chains in each structure unit in $PAGC_8$ played a role of synergistic effect in the molecular aggregation process, but the

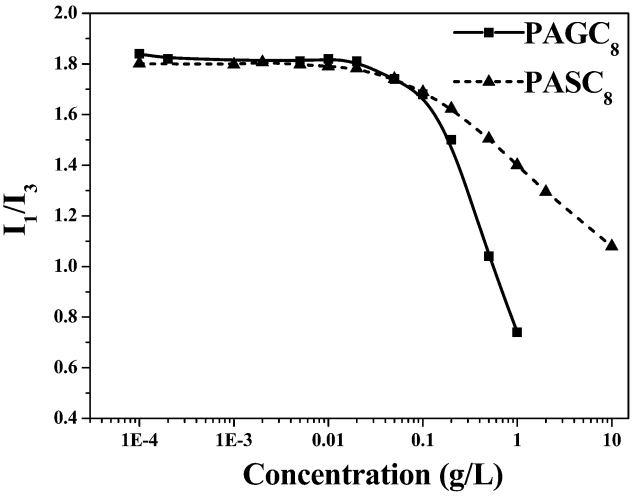


Fig. 2 Fluorescence intensity ratio $I_1/I_3$ curves of homopolymers: $PAGC_8$ and $PASC_8$ in aqueous solution at 25 °C.

high charge density enhanced the repulsion between the homopolymer chains, resulting in little difference of the cac value compared to that of $PASC_8$.

To gain further understanding of the aggregation behaviors, TEM experiments were performed and the images are shown in Fig. 3(I). The aggregate morphologies of $PAGC_8$ were obviously dependent on solution concentration. In dilute aqueous solutions, large complex micelles composed of irregular spherical aggregates were formed. In a high concentration range, they changed to non-continuous network aggregates composed of small spherical micelles of approximately 60 nm interconnected by homopolymer chains, and the accumulation of the network strengthened with the increase of concentration. In the case of $PASC_8$, network aggregates were inclined to form, which showed little dependence on concentration.

As illustrated in Fig. 3(II), in the case of $PAGC_8$, the unique structure with double hydrophobic alkyl chains in each repeat unit brings about synergic hydrophobic effects in the process of self-assembly, while the two charged head groups with close distance enhanced the electrostatic repulsive force, which loosened the aggregate structure and limited the size growth.[25,26] In the low concentration solutions, strong electrostatic repulsion of highly charged head groups may make the molecules leave each other as far as possible, and therefore, the intramolecular hydrophobic interaction is the main driving force for aggregate formation. Further, the interconnections of main chains in molecules make the homopolymer form large spherical aggregates with loose complex structure. In a high concentration range, the main driving force of the self-assembly changes, and the intermolecular hydrophobic interaction plays

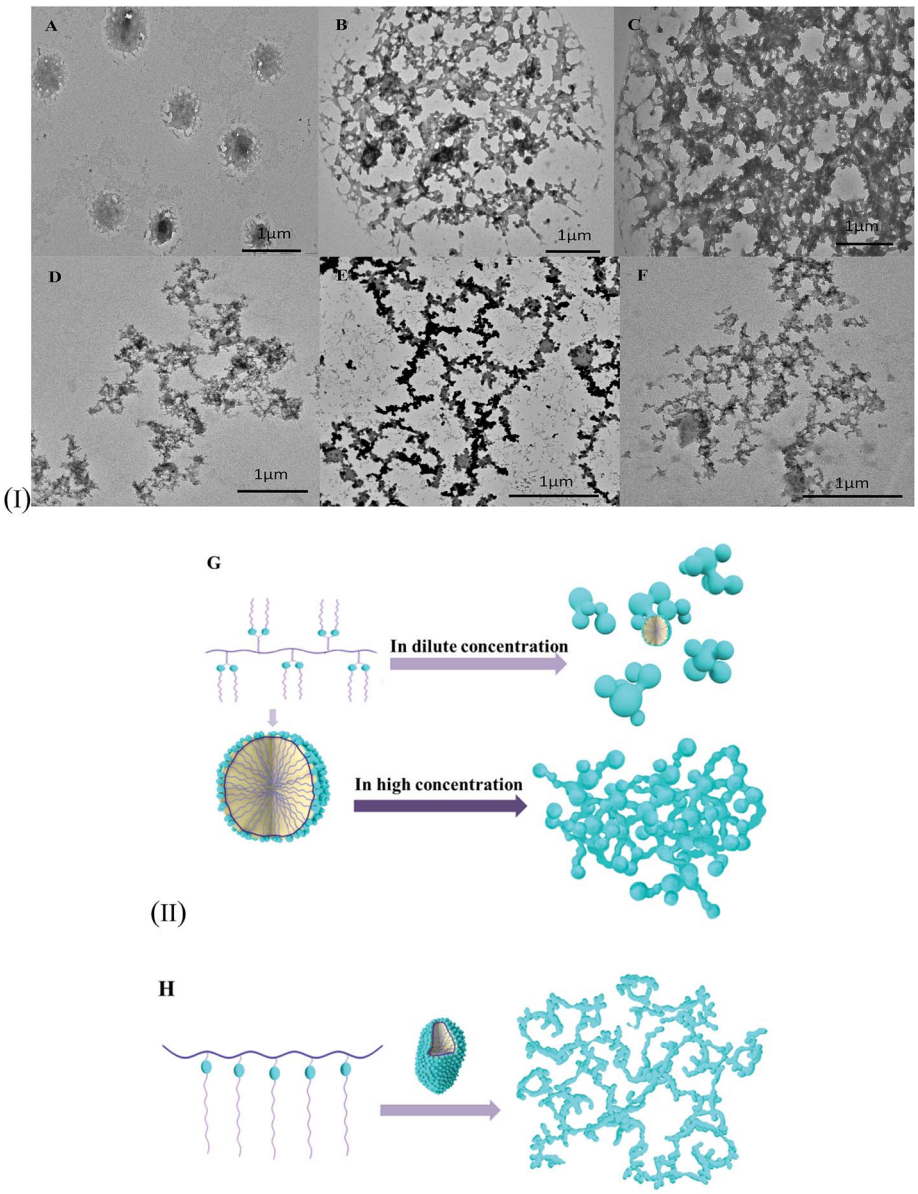


Fig. 3 (I) Typical TEM images of $PAGC_8$ and $PASC_8$ in aqueous solution: (A) $PAGC_8$ 1 g $L^{-1}$, (B) $PAGC_8$ 3 g $L^{-1}$, (C) $PAGC_8$ 5 g $L^{-1}$, (D) $PASC_8$ 1 g $L^{-1}$, (E) $PASC_8$ 3 g $L^{-1}$, and (F) $PASC_8$ 5 g $L^{-1}$; (II) schematic representation of aggregate formation in aqueous solutions for $PAGC_8$ (G) and $PASC_8$ (H).

an important role in forming non-continuous networks which are linked by small spherical micelles. In the case of $PASC_8$, the electrostatic repulsive force is much weaker than that of $PAGC_8$ and, as a result, the intermolecular hydrophobic interaction in any case is the main driving force of aggregate formation, resulting in the formation of networks at the measured concentrations, which is analogous to the performance of $PAGC_8$ in high concentration range.

### 3.2 Environmental dependence of the aggregation behaviors

The self-assembly of amphiphilic polymers has resulted in nanoscale to macroscale morphologies which are of great interest in application areas ranging from materials science to biology. Stimuli-responsive especially environmental response versions of the assemblies are probable to further enhance the scope of flexible applications such as controlled-release materials.[27–29]

It could be found from Fig. 4(I) that vesicles with clear boundaries were formed in the ethanol–water mixed solvents for the $PAGC_8$ system. The formation of vesicles including size and shape was dependent not only on the ethanol–aqueous ratio but also on the concentration of $PAGC_8$. When the ethanol/water ratio increased over 1 : 1, vesicles with different wall thicknesses were formed. Besides, the vesicle sizes could be regulated by the homopolymer concentration. The small vesicles with varied sizes tended to fuse and form large ones in a high concentration range (B and D). The Cryo-TEM images also proved the formation of vesicles in ethanol (E and F). However, the aggregation behaviors of the contrastive structure $PASC_8$ were little dependent on the environment. Only micelles were formed for $PASC_8$ systems at all the values of the ethanol/water ratio range (Fig. 4(II)). The unique aggregation behaviors of the $PAGC_8$ system were also investigated by NMR techniques and will be discussed in the following.

### 3.3 Molecular interaction in the aggregation process

Normally, aggregate transitions have a significant influence on the chemical environment of protons and thus bring about a gradual change in the chemical shifts ($\Delta\delta$).[30,31] Considering the variation of proton signals in different solvents, chloroform-d and a certain amount of acetone in the same capillary were used as external standard.

As shown in Fig. 5, the proton chemical shift of chloroform-d ($H_h$) was adjusted to the same value in order to reduce the deviation caused by different solvents, and the resulting same proton signal value of acetone ($H_g$) indicated that the resonance

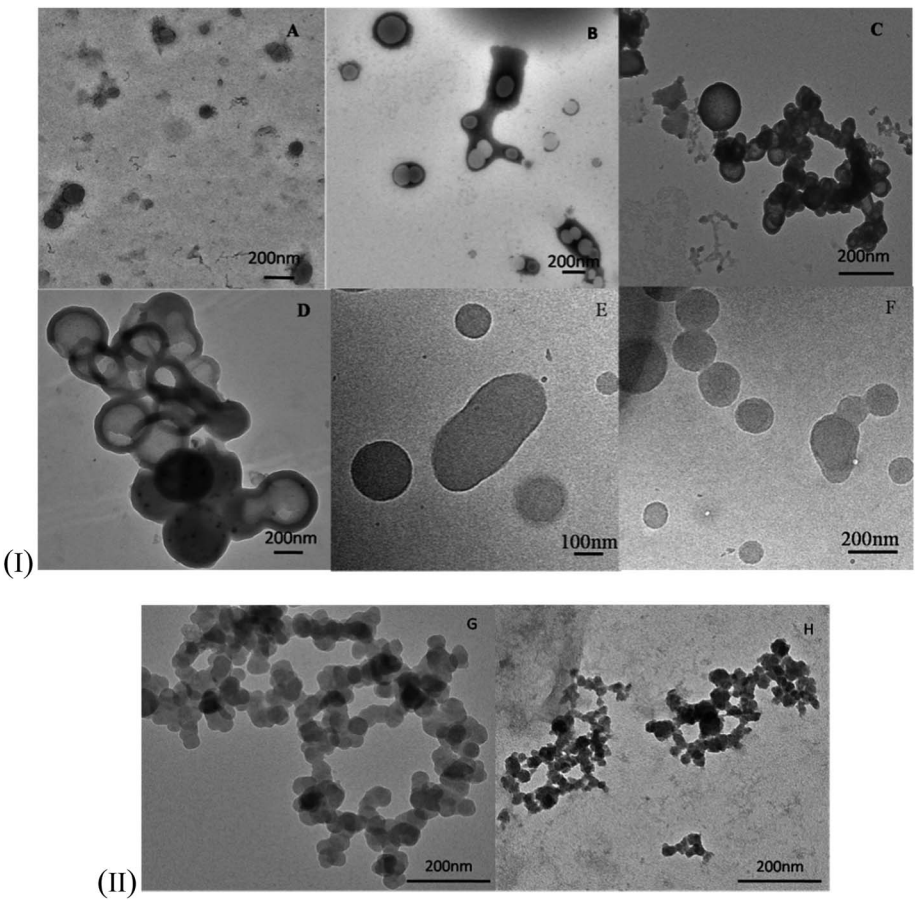


Fig. 4 (I) TEM images of $PAGC_8$ at the concentrations of 1 g $L^{-1}$ and 5 g $L^{-1}$ in ethanol–water mixed solvents (v/v = 1) (A and B) and in ethanol (C and D), and Cryo-TEM images at the concentration of 5 g $L^{-1}$ in ethanol (E and F); (II) TEM images of $PASC_8$ at a concentration of 5 g $L^{-1}$ in ethanol–water mixed solvents (v/v = 1) (G) and in ethanol (H).

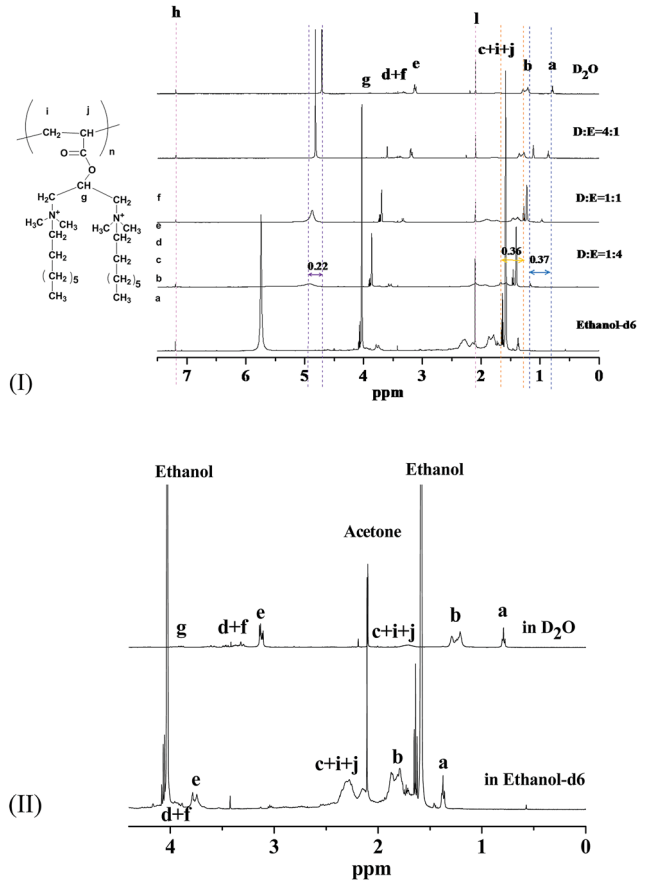


Fig. 5 $^1$H NMR spectra and proton assignments of $PAGC_8$ in different solvents at a concentration of 5 g $L^{-1}$ (I) and part of $^1$H NMR spectra of $PAGC_8$ in $D_2O$ and ethanol-d6 (II).

signals caused by different solvents were ignored. The changes of chemical shifts with micelle formation have been discussed in terms of medium and conformation effects in the literature.[32–34] When the volume ratio of $D_2O$–ethanol-d6 increased from 1 : 0 to 1 : 4, all the chemical shifts of $PAGC_8$ shifted downfield with the addition of ethanol after deducting the solvent effect, as shown in Table 1. Moreover, the protons next to the head groups (quaternary ammonium group) ($H_e$ and $H_{d+f}$) shifted downfield more quickly than those in the tail end of alkyl chains ($H_a$ and $H_b$), which means the decrease of polarity for $PAGC_8$ in such circumstances especially for the head groups. Focusing on the protons b, c (i and j) and e, the peaks split and broadened when the volume ratio of ethanol-d6–$D_2O$ was more than 1, indicating that the surrounding environment for the hydrophilic group changed obviously and the hydrophilic head group rearranged with the transition of the bulk phase.

Further information on the aggregate morphologies can be obtained by the spin lattice relaxation ($T_1$) and spin–spin relaxation ($T_2$). The measurement of proton relaxations is an effective tool for describing the motion and self-association of molecules in solution.[35–37] Spin lattice relaxation depends on the environment of the observed nucleus, which is sensitive to local high frequency motion. However, spin–spin relaxation is sensitive to the slow translational motion of the long chain in the molecule, and the character of this motion is the result of entanglement among long chains. If the value of $T_2/T_1$, defined as $T_R$, is smaller, the correlation time of the molecule motion is longer, and its motility is limited. The $T_2$ and $T_R$ values of the representative protons of $PAGC_8$ ($H_a$, $H_b$, $H_c$ and $H_e$) in different solvents are shown in Table 2. Most values of $T_2$ exhibited bi-exponential behavior at concentrations higher than cac, although they behave exponentially in dilute solutions where aggregation of the surfactant molecules does not occur.[38] As for the former case, values of $T_2$ are obtained by fitting the data to the following equation:

$$M(t) = M(0)[W_f \times \exp(-t/T_{2f}) + W_s \times \exp(-t/T_{2s})]$$

where $W_f$ and $W_s$ stand for the fractions (weighting factors) of protons with fast and slow relaxation, respectively, and $W_f + W_s = 1$. $T_{2f}$ and $T_{2s}$ are the corresponding transverse relaxation times.

As shown in Table 2, the $T_2$ and $T_R$ values of these protons of $PAGC_8$ in $D_2O$ are larger than those of traditional surfactants,[35,38] suggesting more freedom motion for protons. In addition, the $T_R$ values of $H_a$ and $H_b$, which belong to the alkyl chains, are smaller than those of $H_c$ and $H_e$ locating near the head groups ($N^+$), manifesting more restricted motion for $H_a$ and $H_b$ compared with $H_c$ and $H_e$. Herein, the $T_R$ values prove that the aggregates with loose structure have been formed in water, which is consistent with the above conclusion. In mixed solvents, the $T_R$ values are much smaller than those in $D_2O$, suggesting that the motion of these protons becomes more restricted. Especially, the $T_R$ value of $H_e$ is 0.71 in $D_2O$ and 0.33 in ethanol-d6, which indicates that the proton motion becomes restricted in ethanol, meaning a dense packing surrounding the

Table 1 The chemical shift changes of protons of $D_2O$ and $PAGC_8$ of $^1$H NMR when the volume ratio of $D_2O$–ethanol-d6 (D–E) was from 1 : 0 to 1 : 4

| Chemical shifts and their *D*-values | $D_2O$ | $PAGC_8$ | | | | |
|---|---|---|---|---|---|---|
| | | $H_a$ | $H_b$ | $H_{c+i+j}$ | $H_e$ | $H_{d+f}$ |
| $\delta$ (in $D_2O$) | 4.71 | 0.81 | 1.21–1.29 | 1.71 | 3.11–3.13 | 3.31–3.36 |
| $\delta$ (in D–E 1 : 4) | 4.93 | 1.18 | 1.57–1.67 | 1.95–2.11 | 3.53–3.57 | 3.72–3.79 |
| $\Delta\delta$ | 0.22 | 0.37 | 0.36–0.38 | 0.24–0.4 | 0.42–0.44 | 0.41–0.43 |
| $\Delta\delta_{PAGC8}$–$\Delta\delta_{D2O}$ | 0 | 0.15 | 0.14–0.16 | 0.02–0.18 | 0.2–0.22 | 0.19–0.21 |

Table 2 $T_2$ and $T_R$ ($T_2/T_1$) values of $PAGC_8$ in different solvents

| Ethanol-d6 : $D_2O$ | $H_a$ | | $H_b$ | | $H_c$ | | $H_e$ | |
|---|---|---|---|---|---|---|---|---|
| Ratio | $T_2$ | $T_R$ | $T_2$ | $T_R$ | $T_2$ | $T_R$ | $T_2$ | $T_R$ |
| 1 : 0 | 453.6 | 0.32 | 241.64 | 0.47 | 206.73 | 0.47 | 48.54 | 0.33 |
| 1 : 1 | 537.6 | 0.40 | 237.37 | 0.38 | 165.37 | 0.33 | 139.23 | 0.44 |
| 0 : 1 | 1160 | 0.62 | 538.74 | 0.62 | 267.02 | 0.71 | 232.49 | 0.71 |

atoms. It can be inferred that the structures of assemblies in water transfer to more densely packed aggregates in mixed solvents. The transitions in structures in microcosm give better explanation for the changing nature of aggregation behaviors in an ambient environment.

For charged amphiphilic polymers, the subtle and antagonist balance of electrostatic and hydrophobic interactions could lead to a large variety of self-assembly behaviors.[39] In the case of $PAGC_8$, with the increase of ethanol ratio, the side alkyl chains containing the quaternary ammonium groups are strongly exposed to the solvent, but the solvation of the ions becomes much weaker until nearly disappeared, resulting in the decrease of ionization degree, or deionization, which was demonstrated by electric conductivity as shown in Fig. 6.

As mentioned above, the high charge density of $PAGC_8$ played an important role in the aggregation behaviors and the conformation in aqueous solutions. Due to the intervention of ethanol molecules, the bromide ion is not conducive to leave, inducing a low degree of ionization. The oxygen atom of carbonyl, forming a hydrogen bond with ethanol molecules, has a solvophilic effect in ethanol solution, resulting in the changes in the original ratio of electrostatic repulsion as well as the location of hydrophilic head groups. Therefore, $PAGC_8$ tends to form a structure of one head group and two hydrophobic tails in each repeat unit in ethanol solutions (Fig. 7). The structural feature is similar to that of phospholipids with one head group and double hydrophobic tails which is easy to form vesicles.[40,41]

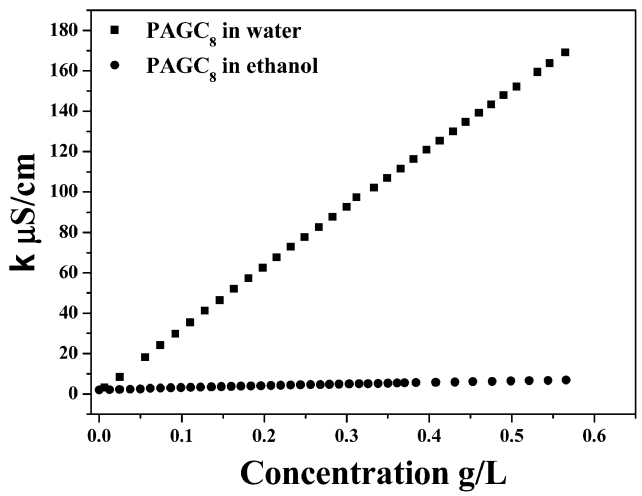


Fig. 6 Conductivity of $PAGC_8$ in water and ethanol solutions measured at 25 °C.

In addition, the aggregate morphology of monomer $AGC_8$ in water and ethanol solutions was observed by TEM (see ESI, Fig. S2 and S3†) which both formed spherical micelles. On these grounds, it could be suggested that the main chain in $PAGC_8$ also played an important role in forming vesicles in ethanol. However, the contrastive structure $PASC_8$ is free from the influence of solvents according to the above results.

The conformation and aggregate morphology transitions presented here provide us significant ideas for designing structure and environmentally responsive soft materials. Particularly, the solvent responsive characteristics make the polymeric assemblies possess a large range of potential applications such as carriers for drugs or cross-linking agents with selective dissolution, nanoreactors, *etc.*

### 3.4 Encapsulation

The ability of the homopolymer $PAGC_8$ to act as a versatile host was determined by encapsulating rhodamine B and Sudan Red, which were used as model hydrophilic and hydrophobic dyes respectively. As shown in Fig. 8, both hydrophilic and hydrophobic molecules were wrapped up in the aggregates, as testified by confocal laser microscopy, and the trapped guest provoked changes in the nature of formed nanoobjects compared with those before trapping. It is worth noting that spherical nanoobjects larger than 200 nm were formed for $PAGC_8$ in aqueous solution after encapsulation (Fig. 8C), whereas, before guest encapsulation, network aggregates composed of small spherical micelles (Fig. 3(I)B and C) existed. In the case of $PAGC_8$ in ethanol, short rod-like aggregates emerged after the embedding process. However, it is interesting

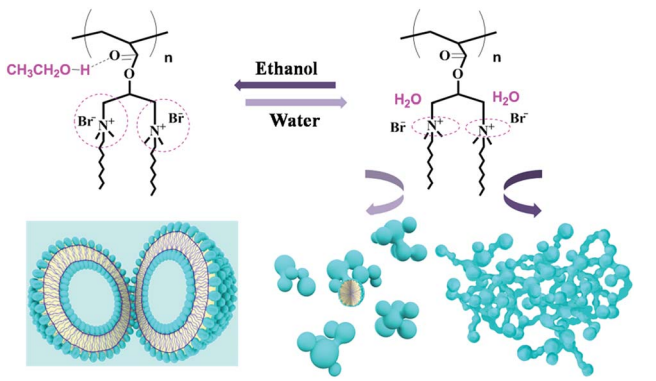


Fig. 7 The aggregate morphologies and structure conformation transition of $PAGC_8$ in ethanol and water.

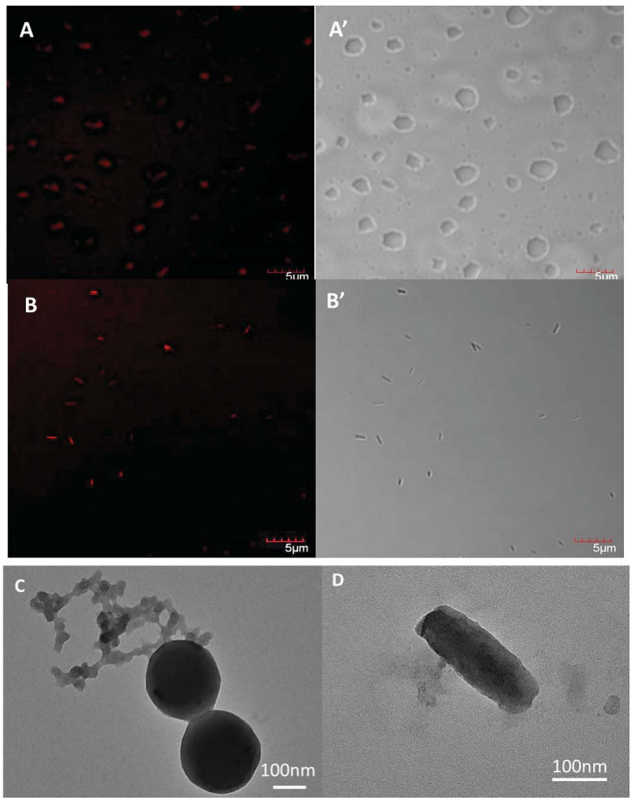


Fig. 8 Representative images of $PAGC_8$ after hydrophilic/hydrophobic dye encapsulation observed by confocal laser microscopy (rhodamine B (A and A′) and Sudan Red (B and B′)) and TEM (rhodamine B (C) and Sudan Red (D)).

to see that the contrastive structure $PASC_8$ showed no efficiency of encapsulation, even with similar aggregates in water. In general, homopolymer $PAGC_8$ with unique structure possessed the capacity to encapsulate the guest.

## 4. Conclusions

Amphiphilic homopolymer $PAGC_8$ with two hydrophilic head and hydrophobic tail groups in each repeat unit has been prepared by aqueous solution polymerization from gemini structure monomers. It was suggested that the self-assembly behaviors of geminized homopolymer $PAGC_8$ were highly dependent on the concentration and media environment. In dilute aqueous solutions, large spherical aggregates with loose complex structure were formed; with the increase of concentration, network aggregates appeared owing to the intermolecular association. With the addition of ethanol, the aggregates transformed to vesicles with clear boundaries, and the wall thickness could be tuned by the water/ethanol ratio. The transition was probably due to the weaker solvation of the polar quaternary ammonium ions in an ethanol environment than that in water, resulting in reduction of the ionization degree and position change of head groups, which changed the electrostatic interaction, conformation and arrangement. The morphology transformation from micelles to vesicles in different environments was highlighted, providing a vivid example of functional smart soft materials with environmentally responsive features. However, the traditional homopolymer $PASC_8$ exhibited monotonous aggregation behavior, invariantly with the environment. Based on these unique behaviors, the possibility of the encapsulating guest was investigated. The $PAGC_8$ had the capacity to encapsulate the hydrophilic/hydrophobic dye depending on the solvents, and, in contrast, the traditional homopolymer $PASC_8$ was incapable of encapsulating dyes, indicating that the novel geminized amphiphilic homopolymer has great potential in preparing environment dependent nanostructures for applications such as in drug containers and other "smart" materials.

## Acknowledgements

The authors are thankful for financial support from the Important National Science and Technology Specific Project of China; "The Application Research on Oil-displacing Agent of Amphiphilic Polymers in Bohai Oilfield" (2011ZX05024-004-03).

## References

1 T. S. Kale, A. Klaikherd, B. Popere and S. Thayumanavan, *Langmuir*, 2009, **25**, 9660–9670.
2 X. Wu, Y. Qiao, H. Yang and J. B. Wang, *J. Colloid Interface Sci.*, 2010, **349**, 560–564.
3 P. C. d. S. Claro, M. E. Coustet, C. Diaz, E. Maza, M. S. Cortizo, F. G. Requejo, L. I. Pietrasanta, M. Ceolín and O. Azzaroni, *Soft Matter*, 2013, **9**, 10899–10912.
4 J. Zhang, Z. Y. Lu and Y. S. Zhao, *Soft Matter*, 2013, **9**, 1947–1954.
5 M. Wang, G. Z. Zhang, D. Y. Chen, M. Jiang and S. Y. Liu, *Macromolecules*, 2001, **34**, 7172–7178.
6 J. Du, H. Willcock, J. P. Patterson and I. Portman, *Small*, 2011, **7**, 2070–2080.
7 Z. Shi, Y. Zhou and D. Yan, *Macromol. Rapid Commun.*, 2008, **29**, 412–418.
8 E. N. Savariar, S. V. Aathimanikandan and S. Thayumanavan, *J. Am. Chem. Soc.*, 2006, **128**, 16224–16230.
9 H. Y. Wang, L. Y. Chai, A. J. Hu, C. X. Lu and B. D. Li, *Polymer*, 2009, **50**, 2976–2980.
10 Y. Q. Zhu, L. Liu and J. Z. Du, *Macromolecules*, 2013, **46**, 194–203.
11 N. Tanaka, *et al.*, *J. Chromatogr. A*, 1999, **836**, 295–307.
12 A. Laschewsky, *Adv. Polym. Sci.*, 1995, **124**, 385–471.
13 S. Basu, D. R. Vutukuri and S. Thayumanavan, *J. Am. Chem. Soc.*, 2005, **127**, 16794–16795.
14 S. Arumugam, D. R. Vutukuri, S. Thayumanavan and V. Ramamurthy, *J. Am. Chem. Soc.*, 2005, **127**, 13200–13206.
15 E. N. Savariar, S. V. Aathimanikandan and S. Thayumanavan, *J. Am. Chem. Soc.*, 2006, **128**, 16224–16230.
16 S. R. Mane, V. Rao, K. Chaterjee, H. Dinda, S. Nag and R. Shunmugam, *Macromolecules*, 2012, **45**, 8037–8042.
17 X. Zhou, X. D. Li, T. Mao, J. X. Zhang and X. H. Li, *Soft Matter*, 2011, **7**, 6264–6272.

18 Y. Wang, C. Y. Ke, C. W. Beh, S. Q. Liu, S. H. Goh and Y. Y. Yang, *Biomaterials*, 2007, **28**, 5358–5368.
19 A. R. Song, S. G. Walker, K. A. Parker and N. S. Sampson, *ACS Chem. Biol.*, 2011, **6**, 590–599.
20 R. Q. Li, L. B. Wei, C. C. Hu, C. F. Xu and J. B. Wang, *J. Phys. Chem. B*, 2010, **114**, 12448–12454.
21 K. Nagai and Y. Ohishi, *J. Polym. Sci., Part A: Polym. Chem.*, 1994, **32**, 445–449.
22 T. S. Kim, T. Hirao and I. Ikeda, *J. Am. Oil Chem. Soc.*, 1996, **73**, 67–71.
23 M. Wilhelm, C. L. Zhao, Y. Wang, R. Xu, M. A. Winnik, J. L. Mura, G. Riess and M. D. Croucher, *Macromolecules*, 1991, **24**, 1033–1040.
24 I. Astafieva, X. F. Zhong and A. Eisenberg, *Macromolecules*, 1993, **26**, 7339–7352.
25 R. Zana, *J. Colloid Interface Sci.*, 2002, **248**, 203–220.
26 Y. Fan, Y. Hou, J. Xiang, D. Yu, C. Wu, M. Tian, Y. Han and Y. Wang, *Langmuir*, 2011, **27**, 10570–10579.
27 Y. Wang, C. Y. Ke, C. W. Beh, S. Q. Liu, S. H. Goh and Y. Y. Yang, *Biomaterials*, 2007, **28**, 5358–5368.
28 S. Ganta, H. Devalapally, A. Shahiwala and M. Amiji, *J. Controlled Release*, 2008, **126**, 187–204.
29 K. Kataoka, A. Harada and Y. Nagasaki, *Adv. Drug Delivery Rev.*, 2001, **47**, 113–131.
30 P. Mukerjee, K. J. Mysels and C. Dulin, *J. Phys. Chem.*, 1958, **62**, 1390–1396.
31 G. Biresaw, D. C. McKenzie, C. A. Bunton and D. F. Nicoli, *J. Phys. Chem.*, 1985, **89**, 5144–5146.
32 J. Ma, C. Guo, Y. Tang, H. Zhang and H. Liu, *J. Phys. Chem. B*, 2007, **111**, 13371–13378.
33 T. Brand, E. Cabrita and S. Berger, *Prog. Nucl. Magn. Reson. Spectrosc.*, 2005, **46**, 159–196.
34 S. Shimizu, P. R. Pires and O. A. El Seoud, *Langmuir*, 2003, **19**, 9645–9652.
35 B. O. Persson, T. Drakenberg and B. Lin dman, *J. Phys. Chem.*, 1976, **80**, 2124–2125.
36 T. W. Davey, W. A. Ducker and A. R. Hayman, *Langmuir*, 2000, **16**, 2430–2435.
37 X. Huang, Y. Han, Y. Wang and Y. Wang, *J. Phys. Chem. B*, 2007, **111**, 12439–12446.
38 S. Zhao, H. Z. Yuan, J. Y. Yu and Y. R. Du, *Colloid Polym. Sci.*, 1998, **276**, 1125–1130.
39 A. V. Subbotin and A. N. Semenov, *Polym. Sci., Ser. C*, 2012, **54**, 36–47.
40 Q. L. Yang, Y. Q. Guo, L. H. Li and S. W. Hui, *Biophys. J.*, 1997, **73**, 277–282.
41 Y. Fang and D. G. Dalgleish, *Langmuir*, 1995, **11**, 75–79.